J Am Oil Chem Soc (2011) 88:1211–1221
DOI 10.1007/s11746-011-1768-1

ORIGINAL PAPER

Synthesis and Characterization of Corn Oil Polyhydroxy Fatty Acids Designed as Additive Agent for Many Applications

R. E. Harry-O'kuru · A. Mohamed · J. Xu · B. K. Sharma

Received: 2 August 2010 / Revised: 3 January 2011 / Accepted: 17 January 2011 / Published online: 18 February 2011

Abstract Before the advent of the modern food industry, vegetable oils (triglycerides) from many sources had a long history of use as condiments in cooking, personal care, and other therapeutic applications. Industrial applications of vegetable oils outside of food usage, on the other hand, have been limited on account of the shorter shelf-life durability of these oils resulting from the natural unsaturation (carbon–carbon double bonds) in the structure of most triglycerides. In seeking to explore expanded utilization of this renewable resource, we have eliminated the above weakness by chemically modifying the double bonds in the material in an attempt to stabilize the oil. We have used FT-IR and NMR spectroscopy to characterize the derivative whereas the physical and chemical properties of the product in terms of stability and flow characteristics have been investigated using differential scanning calorimetry (DSC), pressure DSC, rheometry and thermogravimetric analysis. In this modification of corn oil the data obtained indicate that the resulting poly-hydroxylated acids are more stable than the native corn oil. Additionally, the obtained properties are unique and such that this product will be amenable to use in cosmetics, pharmaceuticals, and other industrial uses especially as a lubricity enhancing additive in fuel applications.

Keywords Corn oil · Epoxidation · Corn polyhydroxy triglycerides · Corn polyhydroxy fatty acids · DSC · Pressure DSC · Rheometry · Thermogravimetric analysis

Names are necessary to report factually on available data. The USDA neither guarantees nor warrants the standard of the product, and the use of the name by USDA implies no approval of the product to the exclusion of others that may also be suitable.

R. E. Harry-O'kuru (✉)
Bio-Oils Research Unit, National Center for Agricultural Utilization, United States Department of Agriculture-Agricultural Research Service, 1815 N. University Street, Peoria, IL 61604, USA
e-mail: Rogers.HarryOkuru@ars.usda.gov

A. Mohamed · J. Xu
Plant Polymer Research Unit, National Center for Agricultural Utilization, United States Department of Agriculture-Agricultural Research Service, 1815 N. University Street, Peoria, IL 61604, USA

B. K. Sharma
Illinois Sustainable Technology Center, University of Illinois, Urbana-Champaign, 1 Hazelwood Dr., Champaign, IL 61820, USA

Introduction

From the time of Predynastic Egypt through to the modern highly mechanized agricultural practices in the United States and elsewhere, corn (*Zea mays* L.) has always played a key role in the livelihood of human populations. It has served as a food as well as condiment source for man and his animals. Like most seeds the corn kernel contains a sizable amount of edible oil that has been exploited over the years mainly for cooking and sometimes as a component in home-made therapeutic remedies. This oil is mainly a C-18 triglyceride with profile as shown in Table 1. Like castor oil, (the gold standard of vegetable oils, for until recently castor was the only naturally hydroxylated vegetable oil) the role of corn and other vegetable oils is dramatically expanding into territories that were hitherto the preserve of petroleum-based oils, i.e., fuels and industrial lubricants, etc. The new interest and thrust into these areas of utilization of vegetable oils is a result of two nudging influences: the

Table 1 Fatty acid composition of corn oil

Fatty acid composition	%[a]
12:0	0.0–0.3
14:0	0.0–0.3
16:0	10.7–16.5
16:1	0.0–0.3
18:0	1.6–3.3
18:1	24.6–42.2
18:2	39.4–60.4
18:3	0.7–1.3
20:0	0.3–0.6
20:1	0.2–0.4
20:2	0.0–0.1
22:0	0.0–0.5
22:1	0.0–0.1
24:0	0.0–0.4

[a] Literature values

public awareness and insistence for the need to save our environment from the pollution caused by use of non-degrading petroleum-based products and the escalating cost of these non-renewables as opposed to renewable bio-based products that are more environmentally friendly. Many years ago it was not economical to even think in terms of transforming vegetable oils into industrial fuels and lubricants but the rising cost of petroleum products particularly the specter of untold environmental disasters of incalculable cost and the uncertainty of their continued availability have changed the equation as seen in the increased investment in bioenergy, namely biofuels, solar and wind. Pursuant to this new area of reawakened interest, we have explored the conversion of corn oil to its more stable yet environmentally degradable form, the polyhydroxy fatty acids [1–5]. Fourier transform infrared spectroscopy, (FT-IR) and nuclear magnetic resonance spectroscopy (NMR) were used to study the chemical conversion whereas the investigation of the physical characteristics of the resulting product were performed using differential scanning calorimetry (DSC), pressure DSC, thermogravimetric analysis (TGA) for assessment of its thermal stability and rheometry for flow behavior.

Materials and Methods

Materials

Hydrogen peroxide (50%) and potassium hydroxide were purchased from Sigma-Aldrich (St. Louis, MO, USA) whereas formic acid (99%), hydrochloric acid, sodium chloride and ethyl acetate were from ACRŌS Organics (Chicago, IL, USA). Pure corn oil was purchased from TOPCO Associates LLC (Skokie, IL, USA).

Methods

Synthesis of Epoxidized Corn Oil

Commercial grade pure corn oil (1.721.0 kg, 1.956 mol) was placed in a three-necked, 3-L jacketed reactor equipped with a mechanical stirrer. The oil was vigorously stirred and the jacket heated to 40 °C. Formic acid (99%, 146.4 g, 0.3 equiv/C=C) was then added in one portion followed by dropwise addition of hydrogen peroxide (50%, 560 mL i.e., 9.7 mol). At the end of hydrogen peroxide addition, the temperature was raised to 70 °C while stirring continued and the reaction progress was monitored by FT-IR at hourly intervals [4–8]. A spectrum obtained after 3.5 h indicated that reaction was complete. At that point the heat source was turned off and after cooling to room temperature the reaction mixture was transferred into a 4-L beaker using ethyl acetate as diluent. To this solution was added a saturated solution of NaCl (400 mL) and saturated Na_2CO_3 (50 mL) with stirring. After effervescence had subsided, portions of the mixture were transferred into a separatory funnel in which the phases were separated. The organic layers were combined whereas the aqueous layers were pooled and re-extracted twice with more ethyl acetate. These extracts were added to the organic phase and dried over Na_2SO_4. The dried organic solution was filtered and concentrated at 57 °C under reduced pressure followed by pump vacuum to give 1.849 kg (98.4%) poly-epoxy triglyceride of corn oil. FT-IR of the product on NaCl discs gave ν_{film} cm^{-1}: 2926 very strong (–CH_3, –CH_2– asym. stretch), 2855 very strong (–CH_3, –CH_2– sym. stretch), 1740 very strong (>C=O stretch), 1464 s (–CH_2– deform), 1380 m-s (–CH_3 deform), 1241 m-s (OCO stretch of ester), 1160 very strong (–HCO–), 1107 m-s (–HCO–), 844–824 m doublet (COC epoxy ring asym stretch), 724 m (–CH_2– wag). This is compared to the starting corn oil which film had the following bands cm^{-1}: 3015 m (H–C=C stretch), 2926 very strong (CH_3, CH_2 asym.), 2855 very strong (CH_3, CH_2 sym), 1746 very strong >C=O), 1656 w (C=C puckering), 1464 m (CH_2 deform), 1378 m-w (CH_3 deform), 1238 w-m, 1164 s, 723 w-m. ^{1}H NMR ($CDCl_3$) δ (ppm of epoxide): 5.25 m(1H), 4.28 d ($J =$ 4 Hz, 2H), 4.25 d($J = 4$ Hz, 3H), 4.12 m(2H), 3.08 m(2H), 2.90 m(3H), 2.29 m(7H), 1.72 m(3H), 1.55 bs(8H), 1.45 m(15H), 1.34 m(47H), 0.85 t(9H); ^{13}C NMR ($CDCl_3$) δ (ppm): 173.2, 173.1, 172.7 (–C=O); 68.88 (methine carbon of glycerol backbone), 62.04 (1° Cs of glycerol backbone); 57.14, 57.09, 56.94, 56.88, 56.66, 56.59, 54.28, 54.27, 54.12 (epoxy carbons); 34.08, 33.98, 33.92 (–CH_2– proximal to O–C=O); 31.87, 31.80, 31.61 (C-11 of

the linoleoyl; C-11 and C-15 of the linolenyl); 29.64 (–CH_2–), 29.60 (–CH_2–), 29.56 (–CH_2–), 29.49 (–CH_2–), 29.479 (–CH_2–), 29.41(–CH_2–), 29.37 (–CH_2–), 29.30 (–CH_2–), 29.24 (–CH_2–), 29.21 (–CH_2–), 29.16 (–CH_2–), 29.13 (–CH_2–), 29.11 (–CH_2–), 29.05 (–CH_2–), 28.99(–CH_2–), 28.93 (–CH_2–), 28.90(–CH_2–), 27.85(–CH_2–), 27.83(–CH_2–), 27.78(–CH_2–), 27.75(–CH_2–), 27.17(–CH_2–), 26.88(–CH_2–), 26.56(–CH_2–), 26.53(–CH_2–), 26.51(–CH_2–), 26.41(–CH_2–), 26.40(–CH_2–), 26.19(–CH_2–), 26.08(–CH_2–), 24.80(–CH_2–), 24.75(–CH_2–); 22.63, 22.60, 22.57, 22.51, 22.43 (–CH_2–α- to terminal –CH_3), 14.15, 14.06, 14.04, 14.00, 13.93 (terminal –CH_3s).

Synthesis of the Polyhydroxy Acids of Corn Oil from its Poly-Oxirane Triglycerides

In a 1000-mL, three-necked, round-bottomed flask equipped with a mechanical stirrer and a reflux condenser was placed 200 g (209.3 mmol) of the poly-epoxide from the above reaction. To this pale-yellow viscous oil was added 6 M HCl (250 mL) with stirring and the system was heated to 70 °C overnight. When FT-IR sampling showed no more epoxy functionality at around 820–840 cm^{-1} but rather a pronounced OH stretching mode centered around 3400 cm^{-1}, heating was discontinued and the reaction allowed to cool to room temperature. Finally, KOH (46.0 g, 698 mmol) in ethanol 300 mL was gradually added to the stirring solution and reheated to gentle reflux for about 3 h until IR of a sample of the reaction mixture indicated absence of ester functionality (1740 cm^{-1}) which had been supplanted by the carboxyl stretching mode at about 1708 cm^{-1} in the acidified sample. The reaction pot was then transferred to a Rotovap and concentrated under reduced pressure to remove most of the ethanol at 50 °C. The concentrate was then poured into a large beaker and acidified by titration with concentrated HCl to pH 2–3 when a turbid layer formed above the aqueous phase. This organic material was extracted into ethyl acetate whereas the aqueous layer was re-extracted three more times with aliquots of ethyl acetate until subsequent extracts contained no more color. The combined extract was dried over $MgSO_4$ and concentrated under reduced pressure at 57 °C to give 178.0 g (84.3%) of a very pale yellow material that solidified on cooling. FT-IR spectrum of a neat film of the product on NaCl discs gave ν_{film} cm^{-1}: 3344–2450 b (the carboxylic acid OH stretch overlapping with the 2° alcohol OH groups), 2923 very strong (–CH_3, –CH_2– asym stretch), 2851 s (–CH_3, –CH_2– sym stretch), 1706 very strong (>C=O carboxyl group), 1465 m-s (–CH_2– deform), 1413 m, 1248 m-s (O–C–O carboxyl), 1075 s (H–C–O–), 1030 w (residual ethanol), 937 w, 725 w (–CH_2– wag); ^{1}H NMR ($CDCl_3$) δ (ppm): 6.5 bs (OHs of the 2° alcohols, 10H), 2.31 t ($J = 7.4$ Hz, 7.3 Hz, 10H), 2.06 s (5H), 1.65 t($J = 6.8$ Hz, 7.1 Hz, 15H), 1.45 m (10H), 0.87 t ($J = 5.7$ Hz, 7 Hz, 15H). ^{13}C NMR ($CDCl_3$) δ (ppm): 179.2, 178.9, 178.8, 171.4 (O–C=O carboxylic acid); 84.23, 84.17, 82.91, 82.85, 80.25, 80.18, 79.22, 79.18, 74.57, 74.52, 74.01, 73.97, 73.70, 73.61, 73.06, 71.38 (hydroxylated methine carbons); 38.41, 37.77, 34.08, 34.05, 34.00 (–CH_2– α to the carboxyls), 33.44, 33.37, 32.29, 32.00 (C-11), 31.95, 31.89, 31.85, 31.84, 31.74, 29.66, 29.62, 29.58, 29.54, 29.49, 29.

Differential Scanning Calorimetry

Samples were analyzed using a TA Instruments (New Castle, DE, USA) Q2000 DSC. Each sample (30–35 mg) was placed in a stainless steel pan and hermetically sealed. To eliminate their thermal history, corn oil polyhydroxy fatty acid (CPHFA) samples were loaded on the DSC and heated to 80 °C and cooled to −50 °C at rates ranging from 3 to 15 °C/min, incrementing by 2 °C/min according to Ozawa crystallization kinetics [9]. After each cooling cycle, the samples were heated at 10 °C/min to 80 °C, and then cooled with the next heating rate. To ensure that no degradation occurred, this cooling–heating method was repeated on each sample. DSC runs were done in duplicate, where the onset, peak temperatures, and enthalpy of the crystallization peaks were recorded. For the kinetics analysis, the onset and peak temperatures were analyzed using the Ozawa [9] model to calculate E_a.

Thermogravimetric Analysis

TGA was performed using a 2050 TGA (TA Instruments). For decomposition kinetics analysis, each sample (10–20 mg) was heated in a platinum pan under nitrogen atmosphere at three different heating rates 10, 15, and 20 °C/min, for up to 800 °C. This data was analyzed using the TA Advantage Specialty Library software provided by TA Instruments, which is a direct application of ASTM Standard E1641, "Decomposition Kinetics by TGA".

Rheological Measurements

Rheological properties of CPHFA samples were measured with a Rheometrics ARES strain-controlled fluids rheometer (TA Instruments) using a 25-mm diameter plate–plate geometry. The temperature was controlled at 25 ± 0.1, 35 ± 0.1 and 15 ± 0.1 °C, respectively, in the experimental chamber using a water circulation system. Prior to linear dynamic rheological parameter measurements, a strain-sweep experiment was conducted to ensure linear viscoelastic range conditions. Linear viscoelasticity indicates that the measured parameters are independent of shear strains. Below 0.02% of strain, all measured materials in this study were in the linear range. Small-amplitude

oscillatory shear experiments (shear strain = 0.02%) were performed over a frequency (ω) range of 0.1–500 rad/s, yielding the shear storage G′ and loss G″ moduli. The storage modulus represents the non-dissipative component of mechanical properties. Elastic or "rubber-like" behavior is suggested if the G′ spectrum is independent of frequency and greater than the loss modulus over a certain range of frequency [10, 11]. The loss modulus represents the dissipative component of the mechanical properties and is characteristic of viscous flow. The phase shift (δ) is defined by $\delta = \tan^{-1}(G''/G')$, and indicates whether a material is solid ($\delta = 0$), or liquid ($\delta = 90°$), or something in between. Nonlinear rheological measurements were conducted as steady shear in the range of shear rate of 0.1–500 s^{-1}. Each measurement was repeated at least two times with different samples. The relative errors were all within the range of ±12%.

Pressure DSC

The CPHFA samples were analyzed on a TA Instruments 2920 DSC using a pressure cell. This instrument has a maximum sensitivity of 5 mV/cm and temperature sensitivity of 0.2 mV/cm, which makes it fairly accurate in terms of data reproducibility. The module was first temperature calibrated using the melting point of indium metal (156.6 °C) at 10 °C/min heating rate and later at 5, 10 and 15 °C/min to be used in the study. The sample amount has significant impact on the shape and reproducibility of DSC exotherm. Each sample (5–10 mg) was placed in a hermetically sealed pinhole aluminum pan for interaction of the sample with the reactant gas (oxygen). The sample was then placed in the pressure cell chamber and, prior to each run, the sample chamber was purged three times with oxygen. The sample was then run under an oxygen atmosphere using a pressure of 690 kPa (90 psi) with a purge rate of 150 mL/min from the outlet valve. These conditions maintain maximum contact of oxygen with the sample and eliminate any limitation due to oxygen diffusion in the oil medium. However, extreme care was taken to maintain the pressure of the oxygen gas constant. Two kinds of experiments were performed using pressurized DSC (PDSC): temperature ramping and isothermal. In the temperature ramping experiment, CPHFA samples were run at 5, 10, and 15 °C/min heating rates to 300 °C to determine the oxidation onset temperature (OT). The OT is defined as the temperature when a rapid increase in the rate of oxidation is observed in the system. This temperature is obtained from extrapolating the tangent drawn on the steepest slope of the reaction exotherm. A high OT would suggest a high oxidative stability of the sample whereas a lower OT would indicate a thermally unstable sample. For kinetic studies, the inverse of the OT was plotted against log of the heating rate (b). Using linear regression and subsequent data computation, various kinetic parameters were obtained at different heating rates.

After determination of the OT for oxidation using the temperature ramping method, each sample was then run using an isothermal method as follows: after purging the sample chamber, the run was started without oxygen to equilibrate at the isothermal temperature. After 4 min, oxygen was introduced to the sample and the temperature was held constant. The sample was allowed to run until the onset of oxidation was reached. Oxidation induction time (OIT) was then determined similar to OT from this thermogram, which is a plot of heat flow versus time.

Results and Discussion

Corn oil was converted to its poly-oxirane in excellent yield using in situ generated performic acid in a slight modification of the procedure by Findley et al. [1], Klaas and Warwel [2], Gunstone [3] and Harry-O'kuru et al. [4, 5]. The FT-IR spectral analysis of the product was characterized by the absorbance doublet at 824–844 cm^{-1} which is consequent on the disappearance of the H–C=C at 3009 cm^{-1} and the weak puckering bands of the starting olefin at 1658 cm^{-1} (Fig. 1a). This information was confirmed in the ^{13}C NMR of a sample of the product which gave the following nine resonance peaks: 57.14, 57.09, 56.94, 56.88, 56.66, 56.59, 54.28, 54.27 and 54.12 ppm (Fig. 1). These peaks corresponded to absorbances of the epoxy ring carbons [6–8]. The spectra of the starting material obtained from both of these spectral techniques (FTIR and NMR) are usually transparent in these regions (860–800 cm^{-1} in the IR and 60–50 ppm in the ^{13}C NMR, respectively. The CPHFAs were obtained from the above poly-epoxy triglyceride in a one-pot reaction. Using 6 M HCl, ring opening of the oxirane triglyceride was accomplished followed by alkali saponification of the intermediate polyhydroxy triglycerides without pre-isolation of the latter. Complete saponification was indicated when an acidified aliquot of a sample of the reaction mixture had lost its 1740 cm^{-1} band in the IR and had rather acquired a lower frequency absorption band around 1706 cm^{-1} indicative of the free carboxylic acid functionality. The IR spectral characteristics of the isolated CPHFA are shown in Fig. 1a. In contrast to the starting oil, one of the two characteristics of the CPHFAs is the elevation of the region of the spectrum between 3500 and 2400 cm^{-1} which includes both the alcohol (OH stretch) as well as the alkyl (2900–2800 cm^{-1}) bands. Secondly, there is the observed disappearance of the ester carbonyl band ($\sim$1745 cm^{-1}) of the triglyceride which had given way to the carboxyl carbonyl at about 1705 cm^{-1}. Figure 1c shows the ^{13}C DEPT spectrum of the

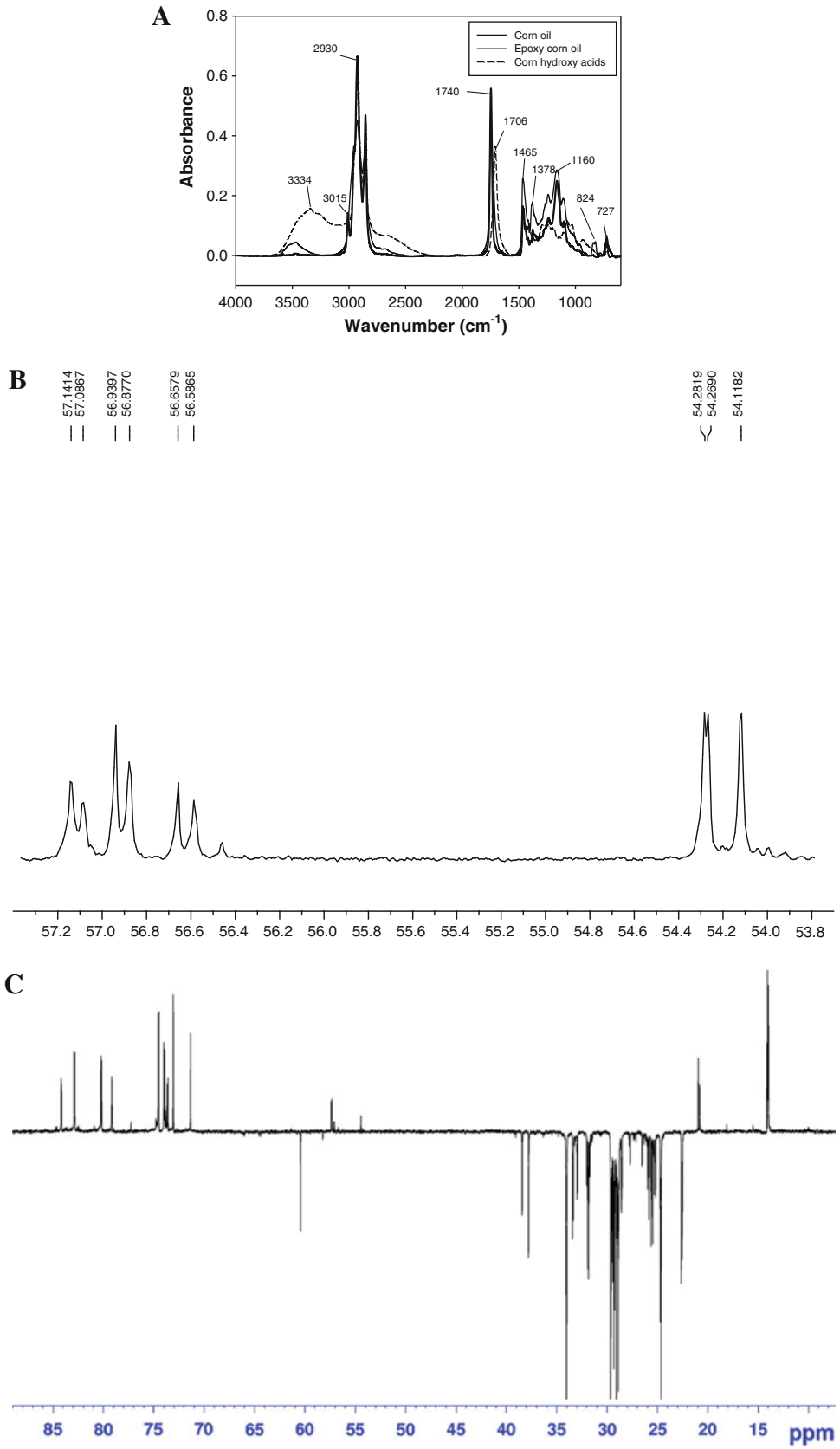

Fig. 1 **a** FT-IR spectrum corn oil polyhydroxy fatty acids overlaid on the unmodified oil and its epoxidized derivative. **b** ^{13}C NMR of corn oil epoxy carbon resonances (58–54 ppm). **c** ^{13}C DEPT spectrum of corn oil polyhydroxy fatty acids

CPHFAs. Significantly, the ten resonance signals corresponding to the ten hydroxylated methine carbons are chemically shifted downfield to 84.05, 82.91, 82.85, 80.24, 74.57, 74.52, 74.03, 73.97, 73.08 and 71.39 ppm compared to the unsubstituted methylene carbons that all occur upfield between 38.43 and 22.58 ppm in the spectrum of the CPHFAs. The other signals of these compounds not usually observed in the DEPT spectrum are the quaternary carboxyl carbons; these resonate farther downfield at 179.15, 178.91, 178.84, and 171.35 ppm. There are, however, two anomalous resonances in this spectrum; the signal at 62.45 ppm (–CH_2O–carbon) and the one at 20.99 ppm (–CH_3) are attributable to residual ethanol left over from the saponification solvent. The data therefore show the conversion of corn oil to its poly-hydroxylated fatty acids.

The value of activation energies (E_a) of polymers can be determined by DSC according to Ozawa [9], when maximum reaction rate temperature is presumed to be the same as peak temperature determined by DSC in non-isothermal conditions. The reaction rate for a solid reactant to produce a solid product can be expressed as:

$$\frac{dx}{dt} = Ze^{-E_a/RT}(1-x)^n \quad (1)$$

where x fraction reacted, Z pre-exponential factor, n reaction order, E_a activation energy, T absolute (K) temperature and R universal gas constant. If the temperature of a first order reaction ($n = 1$) was raised constantly by β and $T = T_p$ (T_p is DSC peak temperature), Mohamed et al. [10] had shown using Eq. 2 below that it is possible to determine the activation energy from DSC data.

$$\ln\left(\frac{\beta}{T_p^2}\right) = \ln\left(\frac{RZ}{E_a}\right) - \left[\left(\frac{E_a}{R}\right)\left(\frac{1}{T_p}\right)\right] \quad (2)$$

where β constant rate of temperature rise, T_p peak temperature, R universal gas constant (8.314 JK^{-1} mol^{-1}), Z preexponential factor, and E_a activation energy. The natural logarithm transformation was used to linearize the equation. From Eq. 2, the plot of $-\ln(\beta/T_p^2)$ against $1/T_p$ represents a straight line with slope $= R/E_a$, thus the activation energy (E_a) value can be calculated ($E_a = R$/slope).

The TGA data can be plotted as temperature versus weight % or temperature versus derivative of weight %, from which the onset and final decomposition temperatures can be obtained as well as the degradation kinetics. Different heating rates are usually used to calculate degradation E_a according to Flynn and Wall [11] based on the following equation

$$\log\beta \cong 0.457\left(-\frac{E_a}{RT}\right) + \left[\log\left(\frac{AE_a}{R}\right) - \log F(a) - 2.315\right] \quad (3)$$

where β is the heating rate, T is the absolute temperature, R is the gas constant, a is the conversion, E_a is the activation energy and A is the pre-exponential factor. According to this equation at the same percent conversion, E_a can be obtained from the slope of the plot of log β versus 1000/T (K). Degradation activation energy was obtained using the software provided by TA Instruments.

CPHFA samples were subjected to heating and cooling cycles using DSC. The cycling revealed a melting peak at 21.0 °C during heating and a crystallization peak at 4.7 °C at 3 °C/min during cooling (Fig. 2). The melting profile exhibited a shoulder right before the main melting peak, indicating variation in the composition of the fatty acids (FAs) contained in the structure of the starting corn triglyceride. It is obvious from Fig. 2 that CPHFA crystallized 16.3 °C lower than its melting temperature, indicating variation in the molecular composition and structure. This variation was also observed in the difference in E_a values during melting and crystallization. The CPHFA structural stability was tested by subjecting the samples to repeated heating and cooling cycles, where the material continued to re-crystallize signifying a highly stable structure under the testing conditions. Higher heating rates caused lower crystallization temperature and ΔH values (Table 2). Although crystallization occurred at a lower temperature, it is evident that a higher heating rate caused structural changes permitting the molecules to crystallize at lower temperature. The system appeared to have less energy as could be deduced from the lower ΔH needed to crystallize compared to melting (Table 2). Overall, the effect of heating rate on the ΔH of crystallization was more evident than that of melting.

The kinetics analysis of melting and crystallization were analyzed using the linearized form of the Ozawa equation [9], where the slope of the straight line was used to

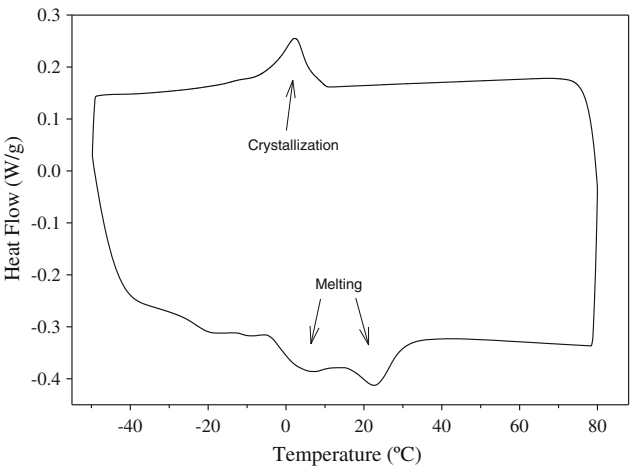

Fig. 2 DSC of corn oil poly-hydroxy fatty acids

Table 2 The ΔH of crystallization and melting

Heating rate	Crystallization ΔH (J/g)	Melting ΔH (J/g)
3	12.01 ± 0.14	14.2 ± 0.19
5	11.70 ± 0.14	13.5 ± 0.23
7	11.10 ± 0.14	13.1 ± 0.52
9	10.92 ± 0.14	12.9 ± 0.11
11	10.51 ± 0.14	12.7 ± 0.43
13	10.25 ± 0.70	12.4 ± 0.09
15	09.79 ± 0.10	12.4 ± 0.17

calculate E_a. The melting kinetics, as described in Table 3 and Fig. 3, exhibited E_a 147.9 (kJ/mol) and 624.2 (kJ/mol) values for the melting onset and peak temperatures, respectively. The large difference between the E_a of onset and peak temperatures (477 kJ/mol) is another indication of the presence of polymorphs in this sample, where some FAs started melting before others causing the significant variation in E_a values. Crystallization kinetics of CPHFA showed E_a 126.9 (kJ/mol) and 111.8 (kJ/mol) values for the crystallization onset and peak temperatures, respectively, which was calculated in the same fashion as in Table 3 and shown in Fig. 4. The small difference in E_a of crystallization between onset and peak (15 kJ/mol) indicates the ability of the molecules to crystallize faster. This was expected because the onset temperature signifies the beginning of the crystallization process, where the onset and peak temperatures continue to decrease at higher cooling rates (Fig. 4).

The TGA profile exhibited two major degradation peaks at 280.7, 386.5 °C, and a minor peak at 446.7 °C as shown in Fig. 5. Since the major FA profile of corn oil is dominated by linoleic, oleic, and palmitic acids, one can presume that the three peaks seen on the TGA represent these three FAs (Fig. 5). The degradation E_a of the composites was calculated from the TGA data, where samples were heat-degraded in a nitrogen environment. The linear form of the Flynn–Wall Eq. 3 was used for the calculation, where the slope of the line was the E_a. The equation was

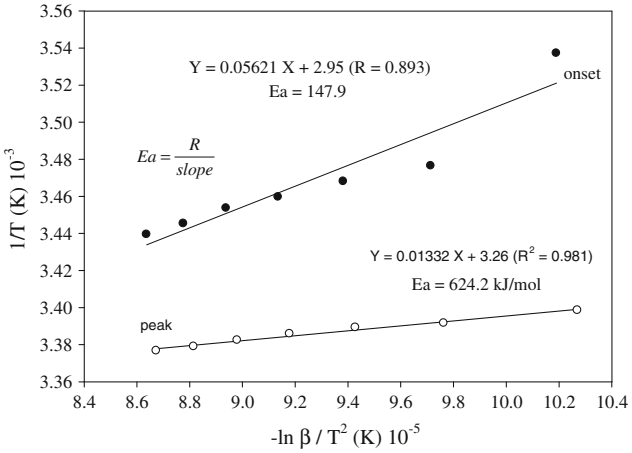

Fig. 3 DSC melting kinetics of CPHFA at heating rate between 3 and 15 °C

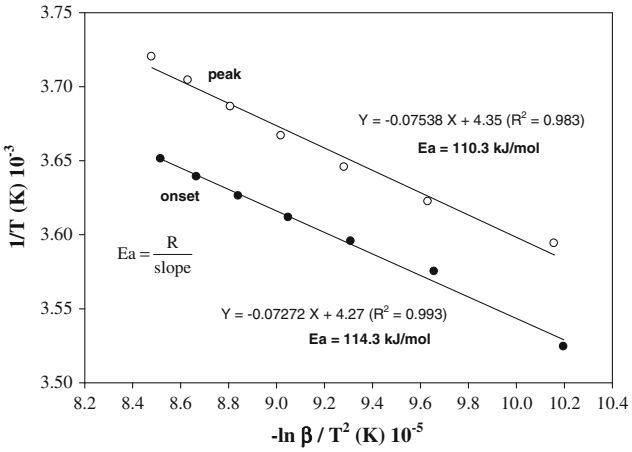

Fig. 4 DSC crystallization kinetics of CPHFA (cooling 3–15 °C)

based on heating samples at different heating rates and the percent degradation–conversion of the material was determined once the weight loss reached between 10 and 90% with an increment of 10%. The degradation mechanism can be determined by plotting the E_a value as a function of percent degradation conversion as shown in Fig. 6. It is

Table 3 Degradation kinetics

Heating rate	T_0 (°C)	T_p (°C)	T_0 (K)	T_p (K)	$1/T_0$ (K) × 10^{-3}	β/T_0^2 (10^{-5}min^{-1}/K^{-1})	$-\ln(\beta/T_0^2)$	$1/T_p$ (K) 10^{-3}	β/T_p^2 (10^{-5} min^{-1}/K^{-1})	$-\ln(\beta/T_p^2)$
3	−6.18 ± 0.18	21.0 ± 0.91	266.97	294.25	3.55	37.54	10.19	3.59	34.65	10.16
5	−5.13 ± 0.23	21.6 ± 0.82	268.02	294.75	3.59	60.43	9.65	3.62	57.51	9.63
7	−3.91 ± 0.14	21.9 ± 0.79	269.24	295.05	3.60	84.19	9.30	3.66	80.41	9.28
9	−3.03 ± 0.14	22.2 ± 0.65	270.08	295.35	3.62	107.72	9.04	3.67	103.17	9.02
11	−2.35 ± 0.22	22.4 ± 0.49	270.80	295.37	3.63	131.20	8.84	3.69	125.85	8.81
13	−1.80 ± 0.17	22.8 ± 0.88	271.35	295.95	3.65	154.31	8.66	3.71	148.42	8.63
15	−1.35 ± 0.13	23.1 ± 0.32	271.80	296.25	3.66	177.44	8.51	3.73	171.03	8.48

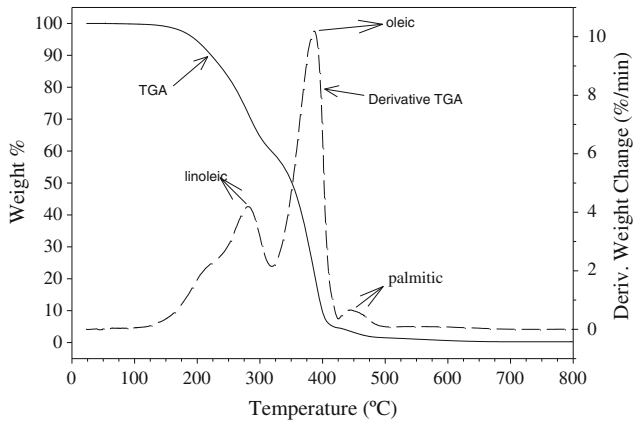

Fig. 5 TGA weight loss % and derivative weight change

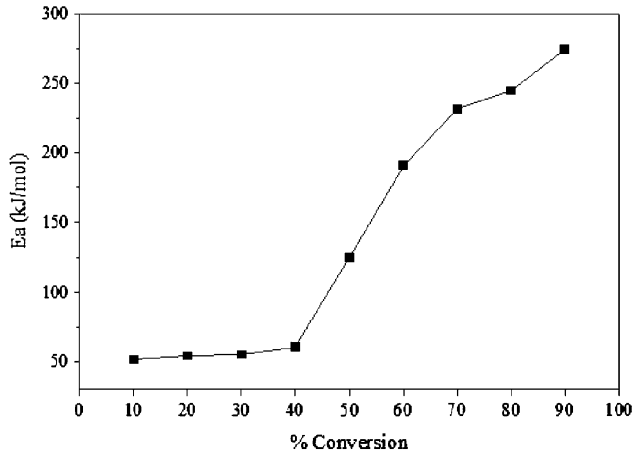

Fig. 6 TGA decomposition kinetics of CPHFA

possible to determine the number of degradation steps from the shape of the line presented in Fig. 6. It is obvious from Fig. 6 that the degradation process reflected a multi-step mechanism indicating the FA composition of CPHFA. In other words, heating occurring during degradation did not generate new components.

The linear rheological properties of dynamic frequency sweep results for CPHFA at three temperatures are shown in Fig. 7. At 25 °C, the CPHFA material exhibited viscoelastic solid behaviors within most measured range of frequencies, which was evident by the greater storage moduli G′ than loss moduli G″ within the experimental range (Fig. 7). The G′ values for CPHFA at 25 °C were in the range of 1.5×10^3–1.5×10^4 Pa, while the phase shift δ values were in the range of 14.3°–57.8°. At 15 °C, CPHFA displayed stronger viscoelastic solid properties compared to 25 °C. The storage moduli (G′) were greater than the loss moduli (G″) over the whole range of the measured frequencies (Fig. 7). The G′ values at 15 °C were in the range of 3.1×10^4–2.0×10^5 Pa, which were more

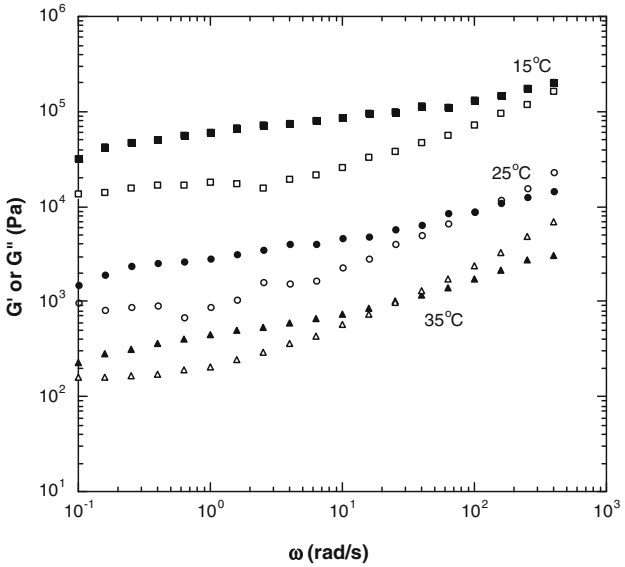

Fig. 7 Dynamic frequency-dependence moduli for CPHFA material at 25, 15, and 35 °C. *Filled symbols* G′, *open symbols* G″. *Circles* 25 °C, *squares* 15 °C, *triangles* 35 °C

than one order higher than those at 25 °C. The phase shift δ values at 15 °C were in the range of 12.3°–39.1°, which were smaller than those at 25 °C. At higher temperature (35 °C), CPHFA exhibited weaker and more fluid-like viscoelastic properties than those at 25 °C and 15 °C. Within more than one-third of the measured frequency range, the loss moduli (G″) were higher than the storage moduli G′ (Fig. 7). The G′ values at 35 °C were in the range of 2.3×10^2–3.1×10^3 Pa, which were about one order lower than those at 25 °C. The phase shift δ values at 35 °C were in the range of 25.3°–66.2°, which were higher than those at 25 °C. These results indicated that the CPHFA exhibited viscoelastic properties like a paste or a weak gel. The obtained rheological properties described above suggests that this material could have potential usage as cosmetic gels or for pharmaceuticals and many other industrial applications.

To understand the functional behavior better, the nonlinear steady shear viscoelastic properties of CPHFA were determined in the 0.1–500 s^{-1} range. Figure 8 shows nonlinear viscoelastic properties of the material at three different temperatures. Under the steady shear measurements, CPHFA exhibited shear-thinning behavior over the entire measured shear rates at all three measured temperatures (Fig. 8). The viscosity was temperature dependent, where higher temperature caused lower viscosity. The shear-thinning rheological behaviors can be characterized by a power law constitutive equation [12]. The power law equation can be written as

$$\eta = K\dot{\gamma}^{n-1} \quad (4)$$

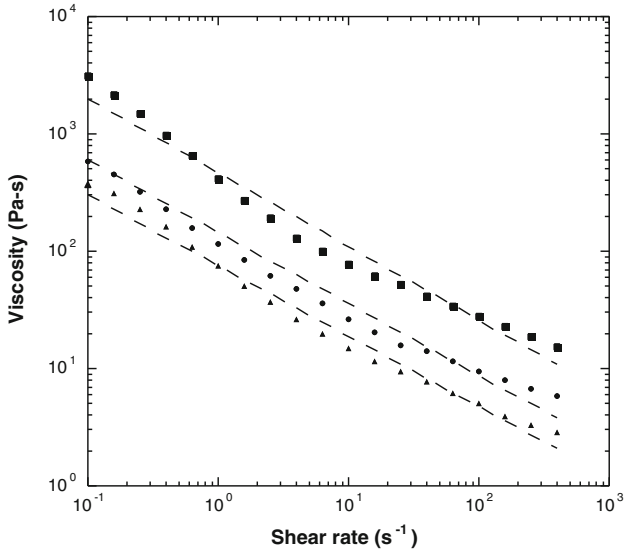

Fig. 8 Nonlinear steady shear viscosities of CPHFA at 25, 15 and 35 °C. *Circles* 25 °C, *squares* 15 °C, *triangles* 35 °C. *Dashed lines* are fitted with power law model

Table 4 Power law model fitted parameters for three temperatures of CPHFA nonlinear rheological properties

Temperature (°C)	K (Pa–s^n)	n	R^2
15	470.7	0.37	0.97
25	145.7	0.39	0.95
35	75.3	0.40	0.98

where η is the shear viscosity, K is the front factor, $\dot{\gamma}$ is the shear rate, and n is the power law exponent. Equation 4 provided a good fit for the shear-thinning viscosity data (Fig. 8) as shown in Table 4. The power law exponents, which indicate extent of the non-Newtonian fluid ($n = 1$ for a Newtonian fluid), were all similar (around 0.4) at three different temperatures (Table 4).

Table 5 shows the variation in (OT) with heating rate during PDSC experiments. The OT shifts to a higher temperature with an increase in the heating rate (b) under constant oxygen pressure (Table 5). The PDSC experiments were carried out using hermetically sealed pinhole aluminum pans and high pressure in these pans allowed rapid equilibration of the oxygen inside the pan. This arrangement effectively eliminated any inconsistency due to access rate of oxygen and egress rate of volatile degradation products. The experiments were performed in the presence of a large excess of oxygen. Therefore, the consumption of oxygen during the oxidation process can be neglected, which means that under this condition the reaction rate is independent of the oxygen concentration and the reaction can be assumed to be first order as long as the oxidation initiation rate is constant. In an earlier study, comparison of the peak areas or enthalpies for aged and fresh peanut oil also confirmed a first-order reaction for the oxidation process [13, 14]. As discussed earlier in melting and crystallization kinetics, the E_a can be calculated using OT as well as the signal maxima (SM) temperatures. In the case of oils, E_a calculated using SM is higher compared to the one calculated using OT, much as in our earlier work on milkweed poly hydroxyl fatty acids (MWPHFAs) [15]. E_a reported using SM is 132 kJ/mol compared to 78 kJ/mol using OT. Such a difference in E_a can be attributed to the composition of oil samples. As these oil samples contain a number of FAs with no hydroxyl, two, four, six hydroxyl groups, etc., this leads to a mixture of components with varied oxidation stabilities. This wide variety of species with different oxidative stabilities may cause one species to start oxidizing before others and may be responsible for the significant variation in E_a values using SM and OT.

In the present work on CPHFAs, OT was used for calculating E_a. The OT observed at each b was converted to the Kelvin values (absolute K) and its inverse was plotted against log b (Fig. 9). The inverse of OT (K) of the CPHFA sample exhibited Arrhenius behavior, as log of heating rate (b) varied linearly with the reciprocal of temperature (K) similar to what has been observed for other oil samples [16, 17]. The slope of the line [δ log b/δ $(1/T)$] was generated from this plot using linear regression. A high coefficient of correlation (R^2 0.99) was obtained for the CPHFA sample. Assuming a first-order reaction for the system during oxidation, the E_a and other kinetic parameters associated with the sample can be calculated using the slope of the line. The E_a was computed using the Ozawa–Flynn–Wall equation (Eq. 5).

$$E_a = -2.19R\,[\delta \log b/\delta\,(1/T)] \tag{5}$$

where R is the gas constant and b is the heating rate (°C/min) used. Assuming a first-order reaction rate, other kinetic parameters could be obtained from E_a for CPHFA. The Arrhenius pre-exponential factor (Z) was calculated from E_a at a specific heating rate b using Eq. 6.

$$Z = \left(b\,E_a\,e^{E_a/RT}\right)\Big/(RT^2) \tag{6}$$

The temperature dependence of specific rate constant (k) can be described by Arrhenius equation 7

$$k = Z\,e^{-E_a/RT} \tag{7}$$

and, the half-life period can then be calculated using Eq. 8

$$t_{1/2} = 0.693/k \tag{8}$$

Table 5 presents the calculated kinetic data of the CPHFA obtained at three heating rates (b) of 5, 10 and 15 °C/min. It was observed that E_a for CPHFA is slightly higher than that for MWPHFA calculated previously using OT. This

Table 5 Calculated values of oxidation kinetic parameters of the corn oil PHFA sample at various heating rates using PDSC

Kinetic parameters	Milkweed PHFA		Corn oil PHFA	
Heating rate (b, °C/min)	10	5	10	15
Onset temperature (T, K)	478	411	421	430
Activation energy (E_a, kJ/mol)	78	80	80	80
E_a/RT	19.6	23.5	22.9	22.4
Arrhenius pre-exponential factor (Z)	1.31E+08	4.43E+09	4.85E+09	4.25E+09
Ln Z	18.69	22.21	22.30	22.17
Specific rate constant (k, min^{-1})	0.41	0.29	0.54	0.78
Half life period ($t_{1/2}$)	1.69	2.43	1.27	0.89

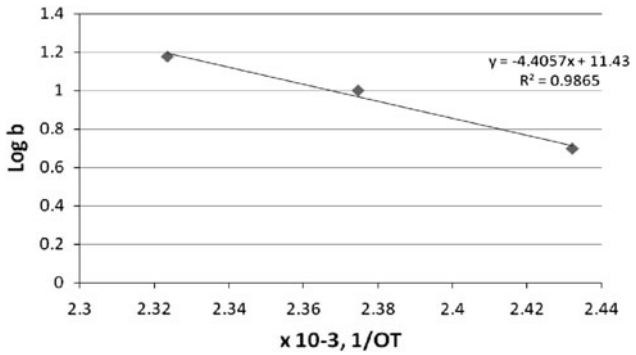

Fig. 9 Plot of inverse of OT (K) versus Log b (heating rate) during PDSC experiments

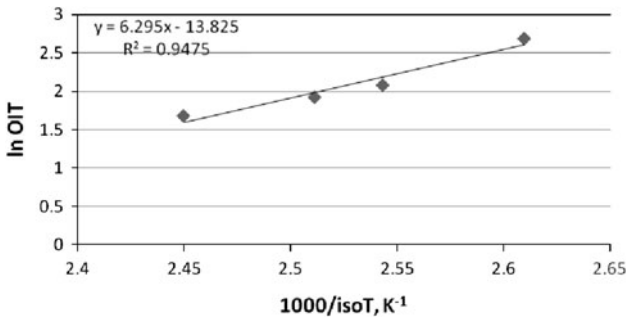

Fig. 10 Plot of inverse of isothermal temperature (K) versus natural log of oxidation induction time during isothermal PDSC experiments

results in subsequent higher values for E_a/RT, Z and k and a lower value for $t_{1/2}$ at a heating rate of 10 °C/min. For CPHFA, the specific rate constant increases, while the half life period decreases linearly with heating rate. The extent of oxidation and formation of oxidation products are further complicated by the amount of residual unsaturation, methylene chain length and other functionalities present in the various molecular species [18, 19]. The cumulative effect of all structural parameters, such as chain length, presence or absence, number and position of hydroxyl groups in the CPHFA makes oxidation a highly complex process and no simple kinetic model alone would hold for such systems.

In vegetable oils, low poly-unsaturation, high mono-unsaturation, and high methylene content increases the E_a for oxidation. In CPHFA, there is no poly-unsaturation as all double bonds have been converted to hydroxylated functionalities. The absence of poly-unsaturation in CPHFA explains the higher E_a requirement and other kinetic data compared to vegetable oils. The OT data show that CPHFAs are less stable to oxidation than MWPHFAs. This early onset of oxidation, where bond scission takes place to form primary oxidation products, may be due to lower methylene content and higher hydroxyl functionalities in CPHFA compared to MWPHFA. These results were also reflected in the higher specific rate constant and lower half life period of CPHFA compared to MPHFA.

Calculated values of E_a and k (Table 5) did not follow the theoretical inverse relation (E_a is directly proportional to inverse of rate constant). The possible reason for this deviation is the large difference in the entropy of complex molecular structures that participate in the oxidation reaction. Oxidation is a very complex process leading to numerous oxidation products involving various intermediates [20]. These intermediate compounds have their own rate constant. The overall E_a is the cumulative effect of all the E_as available in the system during the period of oxidation.

Similar results were obtained in isothermal PDSC experiments. Isothermal PDSC experimental data at different temperatures was also used to calculate the activation energy ($E_{a_{iso}}$). The inverse of isothermal temperature (isoT, K) of the CPHFA sample was plotted against the natural log of OIT (min) as shown in Fig. 10. This plot exhibited Arrhenius behavior, as the natural log of OIT varied linearly with the reciprocal of isothermal temperature (K). The slope of the line [δ ln OIT/δ (1/isoT)] was generated from this plot using linear regression with coefficient of correlation (R^2 0.95) for the CPHFA sample. As mentioned previously, the oxidation reaction of oils is first-order, so, the activation energy ($E_{a_{iso}}$) was calculated

as described in the ASTM D6186-08 standard method using equation (Eq. 9) with R, the gas constant

$$E_{a_{iso}} = R\left[\delta \ln \mathrm{OIT}/\delta\left(1/\mathrm{isoT}\right)\right] \quad (9)$$

The activation energy ($E_{a_{iso}}$) thus calculated for CPHFA is 52.3 kJ/mol is higher than the similar value obtained for milkweed PHFA (24.6 kJ/mol) using isothermal PDSC data. These results corroborate our earlier observation using temperature ramping PDSC experiments, where a higher value of activation energy was obtained for CPHFA compared to MWPHFA. Since the isothermal experiments for these two samples were done at different temperatures, this $E_{a_{iso}}$ value can be utilized to calculate OIT at one temperature for comparison purpose using Eq. 10

$$\mathrm{OIT} = (4.6/k_0) \times e^{E_{a_{iso}}/R\mathrm{isoT}} \quad (10)$$

where OIT is calculated OIT (min), $E_{a_{iso}}$ is activation energy (J/mol) calculated using Eq. 10, k_0 is frequency factor, R is universal gas constant, and isoT is desired isothermal temperature in K. The frequency factor (k_0) was calculated using Eq. 11 for all isothermal temperatures

$$k_0 = (4.6/\mathrm{OIT}) \times e^{E_{a_{iso}}/R\mathrm{isoT}} \quad (11)$$

An average of all values was then used in calculating OIT at the desired temperature using Eq. 10. Using the $E_{a_{iso}}$, k_0 and the desired isothermal temperature of 413.2 K (140 °C), oxidation induction time for corn oil PHFA was calculated at 140 °C. The predicted OIT value for CPHFA at 140 °C is 4.08 min compared to OIT value available for milkweed PHFA (7.32 min) at 140 °C. This again confirms earlier observation that corn oil PHFA is oxidatively less stable than milkweed PHFA.

Acknowledgments The authors wish to express thanks to Dr. Karl Vermillion for the NMR spectra. Our appreciation also goes to Jason Adkins and Mark Klokkenga for technical assistance.

References

1. Findley TW, Swern D, Scalan JT (1945) Epoxidation of unsaturated fatty materials with peracetic acid in glacial acetic acid. J Am Chem Soc 67:412–414
2. Rusch gen Klaas M, Warwel S (1996) Chemoenzymatic epoxidation of unsaturated fatty acid esters and plant oils. J Am Oil Chem Soc 73:1453–1457
3. Gunstone FD (1993) The study of natural epoxy oils and epoxidized vegetable oils by 13C nuclear magnetic resonance spectroscopy. J Am Oil Chem Soc 70:1139–1144
4. Harry-O'kuru RE, Holser RA, Abbott TP, Weisleder D (2002) Synthesis and characterization of polyhydroxy triglycerides from milkweed oil. Ind Crops Prod 15:51–58
5. Harry-O'kuru RE (2005) 4-Hydroxy-3-methoxycinnamate esters of milkweed oil: synthesis and characterization. Lipids 40: 1179–1183
6. Harry-O'kuru RE, Gordon HS, Biswas A (2005) A facile synthesis of aminohydroxy triglycerides from new crop oils. J Am Oil Chem Soc 82:207–212
7. Harry-O'kuru RE, Mohamed A, Abbott TP (2005) Synthesis and characterization of tetrahydroxyjojoba wax and ferulates of jojoba oil. Ind. Crops Prod 22:125–133
8. Ayorinde FO, Butler BD, Clayton MT (1990) *Vernonia galamensis*: a rich source of epoxy acid. J Am Oil Chem Soc 67:844–845
9. Ozawa T (1970) Kinetics analysis of derivate curves in thermal analysis. J Therm Anal 28:301–324
10. Mohamed Abdellatif, Gordon SH, Harry-O'kuru Rogers E, Palmquist Debra E (2005) Phospholipids and wheat gluten blends: interaction and kinetics. J Cereal Sci 41:259–265
11. Flynn JH, Wall LA (1966) A quick direct method for the determination of activation energy from thermogravimetric data. Polym Lett 4:323–326
12. Bird RB, Armstrong RC, Hassager O (1987). Dynamic of polymeric liquids. Wiley, New York, pp 208–209
13. Litwinienko G, Kasprzycka-Guttman T, Jarosz-Jarszewska M (1995) Dynamic and isothermal DSC investigation of the kinetics of thermooxidative decomposition of some edible oils. J Therm Anal Calorim 45:741–750
14. Litwinienko G, Daniluk A, Kasprzycka-Guttman A (1999) Differential scanning calorimetry study on the oxidation of C12–C18 saturated fatty acids and their esters. J Am Oil Chem Soc 76:655–657
15. Harry-O'kuru RE, Mohamed A, Gordon SH, Xu J, Sharma BK (2010) Synthesis and characterization of the intrinsic properties of milkweed polyhydroxy fatty acids. J Am Oil Chem Soc 87:681–688
16. Ferry FD (1980) Viscoelastic properties of polymers, 3rd edn. Wiley, New York
17. Kowalski B (1995) Oxidative stabilities of engine oils contaminated by vegetable oil. Thermochim Acta 250:55–63
18. Adhvaryu A, Erhan SZ, Liu ZS, Perez JM (2000) Oxidation kinetic studies of oils derived from unmodified and genetically modified vegetables using pressurized differential scanning calorimetry and nuclear magnetic resonance spectroscopy. Thermochim Acta 364:87–97
19. Moll C, Biermann U, Grosch W (1979) Occurrence and formation of bitter-tasting trihydroxy fatty acids in soybeans. J Agric Food Chem 27:239–243
20. Tian K, Dasgupta PK (1999) Determination of oxidative stability of oils and fats. Anal Chem 71:1692–1698